A comparison between multispectral aerial and satellite imagery in precision viticulture

(Article begins on next page)

16 May 2024

Precision Agriculture

A COMPARISON BETWEEN MULTISPECTRAL AERIAL AND SATELLITE IMAGERY IN PRECISION VITICULTURE

--Manuscript Draft--

A COMPARISON BETWEEN MULTISPECTRAL AERIAL AND SATELLITE IMAGERY IN PRECISION VITICULTURE

Borgogno-Mondino, E.[1], Lessio, A. [1], Tarricone, L. [2], Novello, V. [1], de Palma, L.[3]

([1]) Department of Agricultural, Forest and Food Sciences, Università di Torino, Largo Braccini 2, 10095 - Grugliasco (TO), Italy

([2]) CREA- Consiglio per la Ricerca e l'analisi dell'Economia Agraria - Unità di ricerca per l'uva da tavola e la vitivinicoltura in ambiente mediterraneo - Via Casamassima, 148 Turi (BA)

([3]) Department of the Science of Agriculture, Food and Environment, Università di Foggia, Via Napoli, 25, 71121 – Foggia (FG), Italy

Corresponding author: enrico.borgogno@unito.it; Tel: 011-6705523; Fax: 011-6705516

Abstract

In this work we tested consistency and reliability of satellite-derived Prescription Maps (PMs) respect to those that can be obtained by aerial imagery. Test design considered a vineyard of Moscato Reale sited in Apulia (South-Eastern Italy) and two growing seasons (2013 and 2014). Comparisons concerned Landsat 8 OLI images and aerial datasets from airborne RedLake MS4100 multispectral camera. We firstly investigated the role of spatial resolution in radiometric features of data and, in particular, of NDVI maps and consequently of vigour maps. We first measured the maximum expected correlation between satellite- and aerial-derived maps. We found that, without any pixel selection and spatial interpolation, correlation ranges between 0.35 and 0.60 depending on the degree of heterogeneity of the vineyard. We also found that this result can be improved by operating a selection of those pixels representing vines canopy in aerial imagery and spatially interpolating them. In this way correlation coefficient can be improved up to 0.85 (minimum 0.60) suggesting an excellent capability of satellite data to approximate aerial ones at vineyard level. Prescription maps derived from vigour one demonstrated to be spatially consistent; but we also found that the quantitative interpretation of mapped vigour was not changing in strength according to datasets and time of acquisition. Therefore, in spite of a

1

satisfying consistency of spatial distribution, results showed that vigour strength at vineyard level from aerial and satellite datasets is generally not consistent, partially for the presence of a bias (that we modelled).

Introduction

In the last years, new agricultural practices based on Geomatic techniques have been experimented and, sometimes, successfully entered the operational farming workflow. Nowadays the rapid evolution of new instruments and techniques, and the related cost reduction drive to consider a new deal for precision farming, where the adaptation of cultural practices to spatial and temporal crop/soil variation is the new frontier (Moran et al. 1997; Cook and Bramley 1998). This approach is basically focused on rationalization of field management and maximization of production (Arnò et al. 2005; Delenne et al. 2010; Song et al. 2014). A double benefit is expected: mitigation of crops environmental impact and maximization of farmer's profit. These factors are particularly important in viticulture, where the final product (wine) shows a potentially high added value that can be obtained with on time management decisions based on spatial variability knowledge of vineyards (Bramley et al. 2005; Profitt et al. 2006; Hall et al. 2011; King et al. 2014). Optical remote sensing has already proved to be effective for this task, permitting to monitor vegetation in space and time; particularly in the last decades it has shown its capability for describing some plants biophysical features, such as vigour, that can be used as proxies of fruit/wine quality and expected yield (Johnson et al. 2001; Hall et al. 2002). Many spectral indices obtained from multispectral imagery were proposed, mainly combining the red and near infrared bands acquired by sensors (Bannari et al. 1995; Zhang et al. 2006). Some of them proved to give a consistent estimation of plant vegetative vigour, that can be related to biophysical parameters through regressive mathematical models (Montero et al. 1999; Haboudane et al. 2002). The most widely used spectral index is the Normalized Difference Vegetation Index (NDVI) that demonstrated to be strictly related with some biophysical characteristics (Lanjeri et al. 2001; Johnson 2003), making possible to describe spatial and temporal variation of grapevine quality and production.

Nevertheless vineyards represent a challenge in the application of remote sensing technologies due to the discontinuous nature of grapevine canopies, their moderate cover, and consequently the prominent background and shadow influences on the measured reflectance signal (Dobrowski et al. 2002), which have to be necessarily processed to separate vegetation from background. Once spectral bands are rigorously pre-processed and combined along spectral index formula, one can investigate spatial variability of the index, interpret it and, finally, derive georeferenced prescription maps (hereinafter called PMs) to use for applying viticultural practices at different rate/intensity. The final aim is to tend at homogenizing crop features and maximizing grape quality and quantity, reducing, at the same time, the farming environmental impact and the production cost (Dry 2000; Haselgrove et al. 2000; Petrie et al. 2000).

Remotely sensed data from Unmanned Aerial Vehicle (UAV) and piloted airplane are, at the moment, the most used ones in precision farming. UAV technology is greatly appreciated since it allows to collect images with very high spatial resolution (Rey et al. 2013). This peculiarity minimize commission between vegetated and not-vegetated pixels, potentially permitting an efficient separation that certainly can improve interpretation. Unfortunately, this peculiarity requires that, to image the entire vineyard, a huge amount of tiles is needed and, consequently, have to be mosaicked during orthoimage generation. This operation, from the remote sensing point of view, introduces a not negligible radiometric uncertainty, since original radiometry of tiles is highly altered to recover a convenient spectral homogeneity of the final product. The most of software used for this task apply different colour balance algorithms neglecting any rigorous processing of the original radiometry (image calibration) required to recover surface reflectance, and, therefore, spectral indexes used for agronomic interpretation. Practically this general superficiality in UAV imagery processing determines that: a) generated orthoimages are not radiometrically correct, b) radiometry is not homogeneous over the scene, c) derived spectral indexes values are unusual. These premises drive, at the moment, to be suspicious about the effective potentialities of UAV images for remote sensing in viticulture: we are convinced that, without a further improvement in data radiometric pre-processing, results from this type of imagery is not reliable to describe vegetation biophysical dynamics and monitoring crop status. On the contrary aerial and satellite imagery are generally not affected by these kinds of limitations. In fact, sensor features and flight heights are generally adequate to image the entire vineyard with a single acquisition, guaranteeing radiometric homogeneity for all pixels of the scene. Due to high performance of sensors and chance to acquire images at a specific time without limitation due to cloud coverage, aerial data are probably the best solution to monitor crops, but also the most expensive choice (Matese et al. 2015). Nevertheless, many satellite data at medium/high geometric resolution have been recently made available for free. In particular the NASA (National American Space Agency) Landsat and ESA (European Space Agency) COPERNICUS Sentinel I-II datasets (Malenovský et al. 2012; Frampton et al. 2013) can be considered the reference products for this type of application. It is our opinion that they can give an important contribution in precision farming both at regional and single-field/vineyard level. Satellite platforms in fact, compatibly with cloud cover, can ensure regular acquisitions in time, mandatory for a precision viticulture approach to vineyard management (Bramley 2001; Bramley et al. 2003). Specifically referring to the Landsat 8 mission, in this work, we demonstrate that, based on OLI data, we can generate estimations of vineyard vigour in space and time, consistent with the ones that can be obtained from aerial imagery. In fact, spatial variation may depend on physical environment factors, like soil, topography and climate, that can condition the differential response of vineyard (Jackson 2008) and, a medium resolution level, may be sufficient to map their effect.

Some works have investigated satellite data potential to evaluate changes in vegetation characteristics aimed to applications in precision farming, demonstrating their utility (Thenkabail 2003; Sibanda et al. 2015). It is well known that coarse resolution (Ground Sample Distance, GSD, between 250 and 1000 m) satellite images, like those recorded by TERRA/AQUA MODIS and ENVISAT MERIS sensors, due to their very high temporal resolution (up to 1-2 acquisitions/day), are the most suitable ones to describe phenology of vegetation (Testa et al. 2014). Unfortunately, while working at vineyard/filed level such GSD is not proper. We therefore excluded this type of data from our work focusing on applications where a continuous monitoring of vegetation is not required and occasional acquisitions are enough. In particular we tested data consistency and reliability between aerial and mid-resolution satellite multispectral acquisitions aimed at generating PMs for calibrating differential interventions on the test vineyard sited in Apulia (South-Eastern Italy). Two growing seasons (2013 and 2014) and two acquisitions per season (June and September) were compared. Satellite dataset was acquired by Landsat 8 OLI (Operational Land Imager) sensor, while aerial dataset consisted of four RedLake MS4100 multispectral images (Green, Red, NIR). Both datasets were radiometrically pre-processed and used to generate vigour maps of the vineyard at the observed dates. It is worth to remind that vigour maps are generally the starting point to derive operational PMs useful to drive vineyard differential management at the ground. Satellite-based maps were therefore compared with the correspondent ones from aerial datasets and their consistency tested. This research was run inside the framework of the Research Project "Promotion of Ecologically Sustainable Processes for Valorisation of Agrifood Production in Apulia – ECO_P4" (task "Improvement of sustainability and efficiency of viticultural and oenological practices and valorisation of local vines biodiversity through precision viticulture techniques" led by the University of Foggia) PON02_00186_2866121 Financed by the EU and Italian Government (MiUR, MiSE).

Materials and Methods

Test Area

The test site was a vineyard of about 3.7 ha. The wine grape variety was Moscato Bianco, a typical white-berry genotype for the growing area, locally named as Moscato Reale for the DOC designation. The centre of the study area is located at 611895 E, 4548884 N in the UTM 33N WGS84 reference frame. The vineyard (property of Torrevento winery) is representative of those devoted to Moscato Reale production in the highlands extended on cretaceous limestone basement in the central part of the Apulia region. Vines were planted (in 2002) at 1.00 x 2.30 m apart. Average edaphic properties were those of a gravel soil, poor in organic matter and scarce or poor in macro- and micro-elements, except for Fe^{3+} that showed a discreet concentration. Plants were trained to Vertical Shoot Positioned system and cane pruned at 12-13 buds/vine. According to the farm practices, vine canopy was uniformly mechanically topped

4

at the end of June, and no bunch thinning was applied. The vineyard received 300 kg ha^{-1} of organ-mineral fertilizer, as average dose. The irrigation was calibrated according to the seasonal weather. During 2013 growing season, about 600 m^3 ha^{-1} of irrigation water were supplied. This amount is the normal farm annual volume as suggested by historical values of ET$_o$ and pluviometry (Forte et al. 2005); adopted K$_c$ values are those proposed by Allen et al. (1998); RDI (Regulated Deficit Irrigation) was set to 30% ETC as suggested by Romero et al. (2013) for optimal balance among vine vigor-grape yield-wine quality. In 2014, since exceptionally copious rains (68% higher than usual) befall from April to September, only 200 m^3 ha^{-1} of irrigation water were supplied in mid-late August (the warmer and dryer period), corresponding to about 33% of usual seasonal volume. The vineyard produced 12 and 13 t ha^{-1} of grapes, respectively in the two years.

Fig. 1 Study area location: Apulia, South-Eastern Italy. Geographic System: WGS84 - UTM Zone 33N

Aerial Dataset

Four aerial acquisitions were acquired by the airborne RedLake MS4100 high resolution multispectral camera along 2013 and 2014 growing seasons. Sensor was mounted on board of the piloted light aircraft SKY ARROW 650 TC by TERRASYSTEM s.r.l. Technical features of images are reported in Table 1. MS4100 is a high resolution 3-CCD digital multispectral camera for remote sensing applications. Camera Field-of-View (FOV) is 60 degrees, focal length 14.0 mm, physical pixel size 7.4 □m and radiometric resolution 8 bit. Relative flight altitude was about 1000 m ensuring a spatial resolution of about 0.5 m. Images were acquired using the colour-infrared (CIR) MS4100 configuration, providing multispectral images in the Green, Red and Near Infrared (NIR) bands (Figure 2). Times of flights were intended to describe vineyard at fully developed vine canopy stage (end of June/beginning of July) and at grape harvest or pre-harvest one (end of August/beginning of September).

Table 1 Technical features of aerial images used in this study.

Date	Time	Sun elevation (°)	Sun azimuth (°)
20/06/2013	about 09:45:00z	66.908073	134.424940
23/09/2013	about 12:00:00z	45.723776	206.578138
03/07/2014	about 14:00:00z	48.108801	258.621737
10/09/2014	about 10:45:00z	52.003827	201.908168
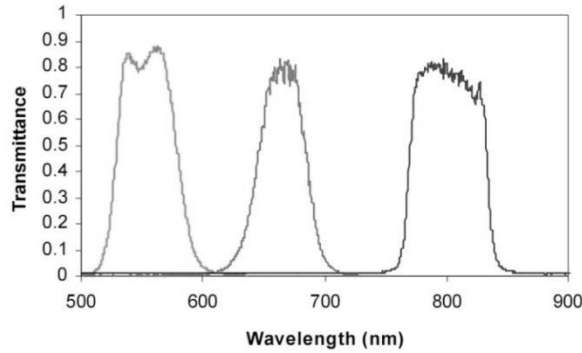
Fig. 2 MS4100 filter design (CIR acquisition mode). Courtesy of TERRASYSTEM s.r.l.

Satellite Dataset

Four OLI Landsat 8 Level 1 data products (hereafter called L8 OLI images) were selected and obtained for free from EarthExplorer distribution system [earthexplorer.usgs.gov/]. Selection was done looking for those L8 scenes whose acquisition date was the closest as possible to the correspondent one of the aerial dataset. Technical features of downloaded satellite images are reported in Table 2.

Panchromatic (band 8), cirrus (band 9) and thermal bands (band 10 and 11) were not considered for this work. Radiometric resolution is 12-bits (rescaled to 16-bits when processed into Level-1 data products) (https://landsat.usgs.gov/sites/default/files/documents/Landsat8DataUsersHandbook.pdf). Table 3 shows acquisition dates and time gaps between the aerial and satellite images.

6

Table 2 Technical features of Landsat 8 OLI images (GSD = Ground Sample Distance).

Scene ID	Acquisition Date	Time	Sun elevation	Sun azimuth	Path	Row
LC81880312013171LGN00	20/06/2013	09:36:45.6624467z	65.66734236	132.1547381	188	31
LC81880312013251LGN00	08/09/2013	09:36:51.4855442z	50.40467477	150.3510512	188	31
LC81880312014174LGN00	23/06/2014	09:34:33.1216337z	65.2684883	130.9534334	188	31
LC81880312014238LGN00	26/08/2014	09:34:54.9808560z	54.20301251	144.9282278	188	31

OLI bands	GSD (m)	Wavelength (nm)	OLI bands	GSD (m)	Wavelength (nm)	OLI bands	GSD (m)	Wavelength (nm)
Band 1	30	433-453	Band 5	30	845-885	Band 9	30	1360-1390
Band 2	30	450-515	Band 6	30	1560-1660	Band 10	100	10600-11200
Band 3	30	525-600	Band 7	30	2100-2300	Band 11	100	11500-12500
Band 4	30	630-680	Band 8	15	500-680			

Table 3 Available images. "I" and "II" are used to identify images respectively acquired at fully developed vine canopy (I) and at the at grape harvest or pre-harvest (II).

	Date	Data source	Time Gap [dd]
I 2013	20/06/2013	Aerial	0
	20/06/2013	Satellite	
II 2013	08/09/2013	Satellite	15
	23/09/2013	Aerial	
I 2014	23/06/2014	Satellite	10
	03/07/2014	Aerial	
II 2014	26/08/2014	Satellite	15
	10/09/2014	Aerial	

Aerial Images Pre-processing

Aerial data were provided "rescaled" at-sensor-radiance calibrated [W·m^{-2}·sr^{-1}·µm^{-1}]. Right scale recovering was done applying equation [1] as suggested by data providers:

$$L_\lambda(x,y) = \frac{DN(x,y)}{300} \tag{1}$$

Where DN(x,y) is the digital number of the raw data. At-sensor-radiance calibrated images were successively atmospherically corrected, based on the Chavez (1996) Dark Object Subtraction (DOS) approach. At-the-ground reflectance was obtained by equation [2] derived by Moran et al. (1992) RTM. In this case the contribution of upwelling transmittance was neglected due to the low flight height.

$$\rho_\lambda(x,y) = \frac{\pi \cdot d^2 \cdot \left[L_\lambda(x,y) - \hat{L}_\lambda^{atm} \right]}{\left[\tau_{\lambda down} \cdot \sin[\beta(x,y)] \cdot I_\lambda + E_{down} \right]} \qquad [2]$$

where ρ_λ is the at-the-ground reflectance value, L_λ is the at-sensor-radiance [W·sr^{-1}·m^{-2}·µm^{-1}] obtained by [1], $\hat{L}_\lambda^{atm}$ is the upwelling atmospheric scattered radiance [W·sr^{-1}·m^{-2}·µm^{-1}], d the Sun-Earth distance coefficient (astronomical units), E_{down} the scattered downwelling contribution (that we assumed equal to $\pi \cdot \hat{L}_\lambda^{atm}$), $\tau_{\lambda down}$ the atmospheric downwelling transmittance, β the sun incidence angle (rad), I_λ the sun irradiance [W·m^{-2}·µm^{-1}] calculated from the experimental Planck emission curve corrected at the Top-of-Atmosphere (Gomarasca 2009). β was assumed constant over the vineyard and equal to the sun elevation angle at the moment of the acquisition, since the topography of the area can be retained flat.

Technical features of RedLake MS4100 bands used during pre-processing are reported in Table 4.

Table 4 RedLake MS4100 bands width features and the correspondent Sun irradiance values.

Band	Centre wavelength [µm]	Band pass [µm]	Irradiance [W·m^{-2}·µm^{-1}]
Green	0.550 ± 0.005	0.040 ± 0.005	1909.0
Red	0.670 ± 0.005	0.040 ± 0.005	1538.0
NIR	0.800 ± 0.005	0.040 ± 0.005	1147.0

Satellite Images Pre-processing

L8 OLI images were calibrated and atmospherically corrected using the complete RTM formulation by Moran et al. (1992), based on a DOS approach (eq. 3):

$$\rho_\lambda(x,y) = \frac{\pi \cdot d^2 \cdot \left[L_\lambda(x,y) - \hat{L}_\lambda^{atm} \right]}{\tau_{\lambda up} \cdot \left[\tau_{\lambda down} \cdot \sin[\beta(x,y)] \cdot I_\lambda + E_{down} \right]} \qquad [3]$$

where ρ_λ is the at-the-ground reflectance value, L_λ is the at-sensor-radiance [W·sr^{-1}·m^{-2}·µm^{-1}] obtained by applying *gain* and *offset* values supplied with L8 OLI images, $\hat{L}_\lambda^{atm}$ is the upwelling atmospheric scattered radiance [W·sr^{-1}·m^{-2}·µm^{-1}] estimated by DOS, d the Sun-Earth distance coefficient (astronomical units), E_{down} the scattered downwelling contribution (that we assumed equal to $\pi \cdot \hat{L}_\lambda^{atm}$), $\tau_{\lambda up}$ and $\tau_{\lambda down}$ are respectively the atmospheric upwelling and downwelling transmittance, β the local sun incidence angle (rad) and I_λ the Sun irradiance [W·m^{-2}·µm^{-1}] calculated according to eq. 4 [*http://semiautomaticclassificationmanual. readthedocs.org/en/latest/Landsat_conversion.html*].

8

$$I_\lambda = \pi \cdot \frac{L_{max}^\lambda}{\rho_{max}^\lambda} \hspace{4cm} [4]$$

where L_{max}^λ is the maximum band radiance value and ρ_{max}^λ the correspondent maximum reflectance value. Both values were obtained from the metadata file (*.MTL) of L8 OLI imagery. Again, for the same reasons as above, β was assumed constant over the vineyard and equal to the sun elevation angle at the moment of the acquisition. τ_λ was considered constant over the scene, equal for both images and just band dependent (Table 5). τ_λ values refer to a summertime mid-latitude low-hazy atmosphere (20 km visibility) according to Fenn et al. (1985).

Table 5 Atmospheric transmittance values for each band given for a reference summertime mid-latitude low-hazy atmosphere.

| L8 OLI band n.	Atmospheric transmittance
1	0.50
2	0.60
3	0.65
4	0.65
5	0.80
6	0.89
7	0.92

Vigour Map Generation

Vineyard vigour is generally intended as the strength of the vegetative behaviour of plants (Winkler et al. 1974). Many works found and modelled some correlations between vigour and other properties of plants and/or grapes (Price and Bausch 1995; Pinter et al. 2003; Johnson et al. 2003; Cortell et al. 2008). In remote sensing, vigour is generally represented by specific spectral indices obtained as mathematical aggregation of bands acquired by multi- or hyper-spectral sensors. Vigour can be investigated at plant level or at vineyard level. According to L8 spatial resolution the first approach cannot be taken into consideration; therefore we tested performances of aerial and satellite data in zoning the vineyard according to the different vigour it expresses in its different parts. Moreover, it was not our intention to explore how spectral indexes can be related to biophysical properties of plants/fruits. Differently, we compared satellite and aerial derived vigour maps at vineyard level, showing how similar PMs can be obtained. As representative of spectral indexes we selected the Normalized Difference Vegetation Index (NDVI), which is probably the most widely used one in for vegetation studies. NDVI can be calculated according to the canonical formulation given by Rouse et al. (1974) [5]:

$$NDVI(x,y) = \frac{\rho_{NIR}(x,y) - \rho_{RED}(x,y)}{\rho_{NIR}(x,y) + \rho_{RED}(x,y)} \qquad\qquad [5]$$

where $\rho_{NIR}(x,y)$ and $\rho_{RED}(x,y)$ are respectively the at-the-ground reflectance in the NIR and RED bands. In our case study NIR and RED are respectively bands 3 and 2 for MS4100 images and bands 5 and 4 for the L8 OLI ones. Since vineyards are characterized by discontinuous surfaces where grapevine canopies is alternated with bare soil (or with a vegetation different from vine foliage), they represent a particularly difficult challenge for medium resolution images; in fact reflectance of each pixel results from the joint contribution of bare soil and grapevine canopy. Nevertheless, one can suppose that, due to the regular texture of vineyards, spectral index differences among pixels are mainly due to their vegetated component. Therefore, we can imagine that these differences can be related to a different strength of grapevines in the different part of vineyard. According to this hypothesis we considered two types of L8-based vigour maps: a) the ones directly derived from the original NDVI values by Nearest Neighbour (NN) oversampling from 15 to 0.5 m; b) the ones obtained by spatial interpolation of the original NDVI values achieved by Thin Plate Spline (TPS) method.

Differently, aerial images, in force of their higher spatial resolution, permit to separate vegetation from background (soil) at pixel level; potentially each single plant behaviour could be investigated. This situation makes possible to map vineyard vigour with a higher accuracy, but it drives the user to preventively recognize and separate vines canopy pixels from the others. For this task we used the "*Local maxima and minima*" tool available in SAGA GIS 2.2.0 over aerial derived NDVI images. This automatic approach permits the user to forget about the selection of an opportune NDVI threshold that, necessarily, has to be changed according to the season. Extraction of canopy pixels determines that spectral continuity of images is broken (Figure 3) and, consequently, a spatial interpolation step has to be done to recover it. For this work, for each aerial image, we tested spatial autocorrelation of extracted canopy pixels by semi-variogram and spatial interpolation was achieved by TPS using a grid size of 0.5 m. It is worth to remind that, for this work, we referred as "NDVI maps" those directly generated by application of [5] to the calibrated images; as "vigour maps" those generated through spatial interpolation (by geostatistic techniques) of distributed points corresponding to the centres of vines canopy pixels.
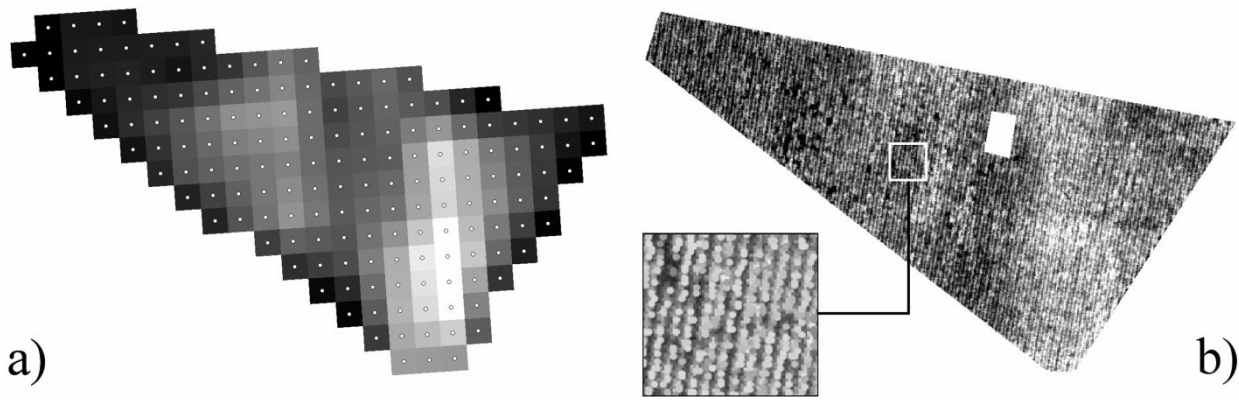
Fig. 3 a) Satellite NDVI map and pixel centers used for spatial interpolation by TPS used to generate SINT05 image. b) Example of aerial NDVI map where vines canopy pixels have been selected by the "Local Minima and Maxima" algorithm of SAGA GIS.

Datasests Comparison: Map Correlation

We firstly compared vigour maps from satellite and aerial datasets for the four acquisitions. Comparisons were achieved at different spatial resolutions, assuming that this is the most important responsible of eventual differences. Comparisons concerned both NDVI and vigour maps. Test design is shown in Figure 4.
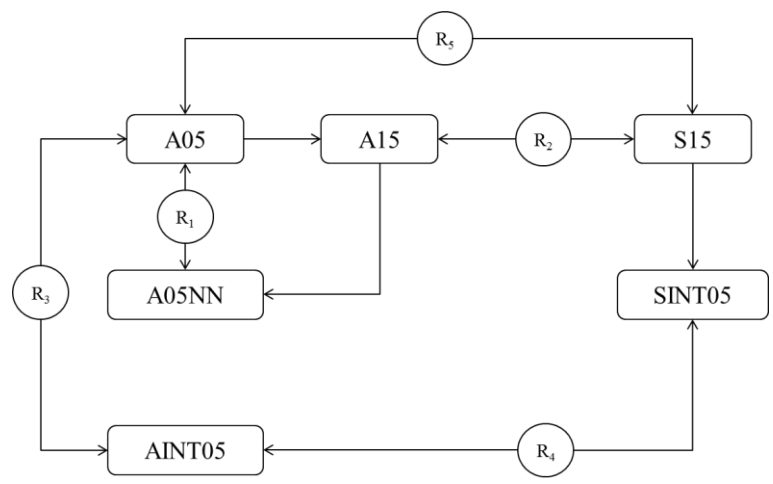
Fig. 4 Experiment design used to test aerial and satellite derived NDVI/vigour maps. Ri are the calculated Pearson's correlation coefficients between compared image, whose meaning is reported in the text.

Preliminarily, we oversampled L8 NDVI images to 15 m to artificially reduce resolution difference between data, making successive comparisons easier by limiting the effects of radiometric borders. Oversampling was performed by bilinear method. A 15 m resolution version of aerial-derived NDVI maps was also generated using the mean value down-sampling method.

Since our main goal was to test aerial versus satellite vigour maps consistency, we selected the Pearson's correlation coefficient as a measure of similarity. Though in literature different approaches are proposed to test maps similarity

11

(Tagarakis et al. 2013) most of them are applied to compare already classified representations (discrete). Since we focused on vigour maps similarity (therefore on continuous representations of a spectral index) these approaches were retained not proper. We admit that, using Pearson's correlation coefficient the absolute strength of signal is neglected and only the relative distribution of values is tested; thus, well correlated datasets could be shifted/scaled of a large amount. We tried to recover this information comparing, in a further step, class statistics of the obtained PMs (see "Results and Discussions", Tables 9 and 10).

The following labels were assigned to aerial-derived products used for comparisons: a) A05 are the aerial derived NDVI maps; b) A15 are the aerial derived NDVI maps down-sampled at 15 m; c) AINT05 are the vigour maps obtained by spatial interpolation (TPS) with a 0.5 m Ground Sample Distance (GSD); d) A05NN are the A15 images resampled back to 0.5 m by NN method. The latter represents the way a sensor with the same features as MS4100, at the same time, would have seen the area with a GSD of 15 m. This, somehow, define the best approximation of the scene that a sensor with a 15 m GSD can generate of the area. The consistency it shows respect to the original 0.5 GSD image can be assumed as the upper limit of correlation we expected from the comparison with L8 OLI imagery.

The following labels were assigned to satellite-derived NDVI/vigour maps used for comparisons: a) S15 are the satellite derived NDVI maps oversampled to 15 m GSD by bilinear interpolation; b) SINT05 are the L8-derived vigour maps generated by spatial interpolation (TPS) from 15 to 0.5 m considering the centres of the S15 pixels. We assume that this data is the best starting point to derive PMs with 0.5 m resolution from satellite imagery. According to the above mentioned labels we tested the following: a) the correlation between A05 and A05NN (R_1) defines the maximum expected similarity that the difference of resolution of the two compared datasets allows. In fact the maximum reachable similarity strictly depends on the difference of spatial resolution of data that are compared. We also investigated the relationship between R_1 and GSD, testing correlation between A05 and many different A05NN obtained by down-sampling A05 to a variable GSD varying between 1 and 30 m with a step size of 1 m (Figure 5); b) the correlation between A15 and S15 (R_2) represents the similarity between aerial and satellite acquisitions at the satellite resolution (15 m); c) the correlation between AINT05 e A05 (R_3) can be used to evaluate the effects of background on vigour maps in aerial acquisitions; d) the correlation between AINT05 and SINT05 (R_4) is probably the most important from an operational point of view, since it measures the similarity between aerial- and satellite-derived vigour maps in the ordinary workflow; e) the correlation between A05 and S15 (R_5) finally was used to test aerial and satellite NDVI maps similarity at the aerial image resolution (0.5 m). A similarity coefficient was defined as the ratio between R_5 and R_1, being R_1 the maximum expected value for the Pearson's correlation coefficient and R_5 the one resulting comparing the original NDVI maps (A05 and S15). Since R_4 values demonstrated (see Results and Discussion paragraph) a satisfying degree of correlation between aerial- and satellite-derived vigour maps, we also tested the

12

strength of differences in terms of vigour values by computing for AINT05 and SINT05 the following statistical parameters: NDVI mean (μ_{NDVI}), standard deviation ($\square_{NDVI}$) and coefficient of variation ($\square\square\square\square\square\square$.

Datasests Comparison: Bias Modelling

Correlation is a statistical operator able to test similarity, but not able to quantify differences between compared datasets. Once correlation is demonstrated (this was the case in our study), it is mandatory to model existing relationship, i.e. bias. We therefore randomly sampled 1000 pixels from AINT05 and SINT05 generating correspondent scatterplots. According to the previously found strong correlation a linear regression model (AINT05 = a*SINT05 + b) was calibrated for each period to correct satellite-derived vigour maps. The calibrated model was then applied to all SINT05 pixels to minimize bias effects and making following comparisons more consistent and reliable.

We tested and measured both vigour differences before and after bias modeling by computing some synthetic statistics (see paragraph "Generation of Prescription Maps"). Absolute value of vigour is, in fact, another important issue to deal with, because the strength of agronomic interventions in the different part of vineyards relies not only on position, but also on the size of mapped vigour differences. This fact turns to be more and more important if vigour maps (or possibly other spectral indices maps) are required to be related to ground surveyed biophysical parameters to calibrate regressive model able to map such parameters over the whole vineyards (Chappelle et al. 1992; Read et al. 2002; Haboudane et al. 2004; Yu et al. 2012).

Generation of Prescription Maps

Vigour maps ordinarily are used to generate PMs useful for operating selectively over the vineyard addressing agronomic interventions aimed at maximizing productivity or, simply, at guaranteeing an homogeneous behaviour of the whole vineyard. From AINT05 and SINT05 vigour maps we derived PMs by clustering. The combined Minimum Distance/Hill-climbing method (Forgy 1965; Rubin 1967) was performed in SAGA GIS, determining, for each vigour map, three different vigour classes. For each cluster the correspondent NDVI mean value was calculated and used to operationally interpret it. We used a vigour distance coefficient (VD) to compare vigour performances of defined clusters (eq. 6) that farmers can easily translate into agronomic drivers.

$$VD = \frac{(\mu_{L/H} - \mu_M)}{\mu_M} \cdot 100 \qquad\qquad [6]$$

13

where μ_M is the mean value calculated for the central cluster and $\mu_{L/H}$ the mean value of the most (H) and less (L) active clusters.

Result and Discussions

Four aerial and four satellite images were calibrated into at-the-ground reflectance value (ρ_λ) using respectively [2] and [3]. Correspondent NDVI and, consequently, vigour maps were calculated from the calibrated bands for all the dates and both the datasets (aerial and satellite) at the original GSD (aerial = 0.5 m, satellite = 30 m). Satellite imagery were therefore oversampled to a 15 m GSD by bi-linear interpolation in order to artificially increment the number of pixels representing vineyard. This operation is specifically achieved to improve spatial interpolation of pixels at a lower GSD (0.5 m). Aerial and satellite maps similarity was tested for all the above described image pairs generating results of Table 6.

Table 6 Correlation coefficients. "I" = fully developed vine canopy period (end of June/beginning of July); "II"= grape harvest/pre harvest period (end of August/beginning of September). R_i meaning: see "Materials and methods" section.

|	R_1	R_2	R_3	R_4	R_5	*Maps similarity [%]*
I 2013	0.48	0.80	0.45	0.81	0.40	82.47
II 2013	0.39	0.80	0.44	0.67	0.33	83.02
I 2014	0.35	0.74	0.32	0.85	0.28	79.71
II 2014	0.58	0.73	0.58	0.60	0.42	73.23

R_1 values show that, generally, the world seen with different GSD by the same sensor at the same time determines not too similar representation ranging between 0.35 and 0.58 depending on the composition of pixels at the moment of the flight, i.e. on the season. This is clearly the effect given by the mixed nature of pixels with higher GSD. R_1 values have to be assumed as the reference upper thresholds of correlation we cannot overcome comparing a 30 m with a 0.5 m GSD acquisitions. Differently, R_2 values are higher (between 0.73 and 0.80) and show that the spectral content of aerial and satellite images at the spatial resolution of satellite (15 m) are very similar. This confirms that, in spite of the time gap between aerial and satellite acquisitions, spectral content persists and can successfully be compared. R_3 values suggest that the contribution of soil spectrum to signal in mixed pixels is significant and it weighs for about 50%.

Focusing on R_4 values (always > 0.6), we can definitely state that spectral information that can be obtained from satellite image well fits, at the vineyard scale, the ones you can get from aerial higher resolution images. In particular, at the start of season aerial and satellite information concerning plants vigour is higher. This suggests that local vegetation activity variations occurring along season in consequence of summer weather generate evidences at the end of season. Since these cannot be detected by satellite we can suppose that the effect of summer induced stresses operates locally at

14

plant scale. R_4 values are the most important ones since they measure aerial- and satellite-derived vigour maps at the highest spatial resolution (0.5 m). This is the one we retain appropriate to investigate vineyard internal variability looking for clusters of vegetative activity to base the extraction of PMs. R_5 absolute values (Table 6) could appear not so encouraging if read without the right interpretative key, given by R_1, that is the maximum value R_5 can reach. For this reasons we used the above mentioned similarity coefficient (SC) as final measure of consistency between aerial- and satellite-derived NDVI maps. Table 6 shows that SC is always above 73%, definitely confirming that L8 OLI images can detect the most of vineyard variability. And, in spite of variations induced locally (at single plant level) from the develop of weather along the growing season of grapevine, the general trend of vineyard performance is correctly detected by satellite imagery. Moreover, SC remains quite stable during the season, demonstrating that seasonality, at vineyard level, can be mapped reasonably with the same consistency in different moments of the season.

Since R_1 is assumed as reference maximum threshold to refer our similarity measures to, we explore its dependence from GSD. We tested 30 different GSD (from 1 to 30 m, with 1 meter step) comparing the original 0.5 GSD aerial images with their down-sampled versions (by Pearson's correlation coefficient). Results are reported in Figure 5, for all the dates. Figure 5 shows that, as expected, R_1 decreases by decreasing image spatial resolution (i.e. higher GSD), but its value, for the same GSD, depends on the acquired scene. In particular, we can say that the factor that strongly conditions this effect is the spatial frequency of mixed pixels. Since during grapevine growing season the ratio between vegetation and soil, within each pixel, varies according to the canopy evolution, we cannot model, once for all, this relationship. Nevertheless, SC values of Table 6 encourage us about the stability of approximation given by lower resolution sensors respect to the higher resolution ones.
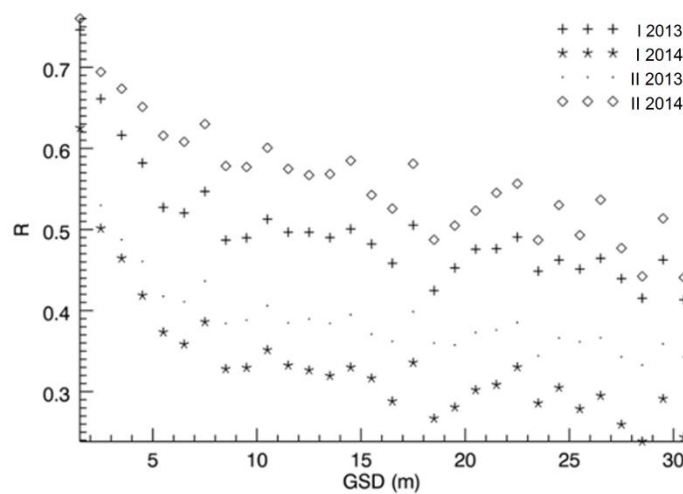
Fig. 5 R1 vs GSD. The role of GSD in conditioning consistency between images acquired at different spatial resolutions; trends refer to the four acquisition dates ("I and "II" like in Table 3).

15

Figure 6 shows final vigour maps. In general, "low frequency" spatial variations of vineyard vigour detected by satellite and aerial sensors are consistent. Aerial-derived maps, naturally, can detect even local variations that satellite is not able to appreciate. Nevertheless, consistency of spatial distribution of vigour is greatly satisfying.

Successively, we calculated some synthetic statistics (Table 7) quantifying differences between aerial- and satellite-derived vigour maps (respectively AINT05 and SINT05) before and after vigour bias modelling: vineyard vigour mean value (μ_{NDVI}), standard deviation (σ_{NDVI}) and coefficient of variation (σ^*).
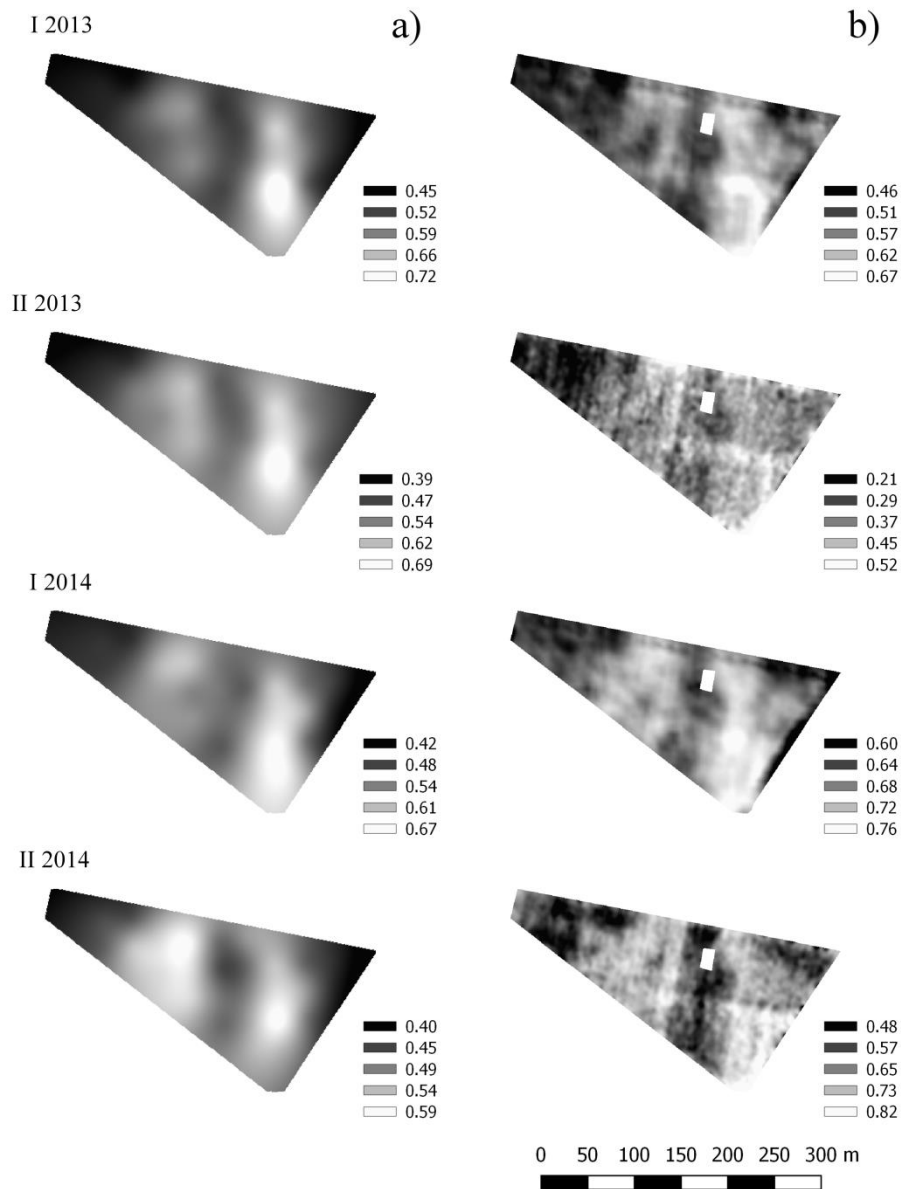
Fig. 6 a) Satellite-derived vigour maps (SINT05). b) Aerial-derived vigour maps (AINT05). Map grey levels (reported in legend) correspond to the interpolated NDVI values ("I and "II"like in Table 3).

16

Table 7 Overall statistics (mean, standard deviation and coefficient of variation) of the compared vigour maps (satellite SINT05 vs aerial AINT05). "I" = fully developed vine canopy period (end of June/beginning of July); "II"= grape harvest/pre harvest period (end of August/beginning of September).

	Aerial (A)			Satellite (S)			S-A	Satellite Corrected (SC-A)			SC-A
	μ_{NDVI}	σ_{NDVI}	σ^*	μ_{NDVI}	σ_{NDVI}	σ^*	$\Delta\mu$	μ_{NDVI}	σ_{NDVI}	σ^*	$\Delta\mu$
I 2013	0.560	0.054	0.096	0.562	0.069	0.123	+ 0.002	0.560	0.042	0.075	+ 0.000
II 2013	0.381	0.076	0.199	0.551	0.074	0.134	+ 0.170	0.376	0.050	0.133	- 0.005
I 2014	0.689	0.045	0.065	0.545	0.064	0.117	- 0.144	0.690	0.037	0.054	+ 0.001
II 2014	0.666	0.091	0.137	0.501	0.051	0.102	- 0.165	0.661	0.055	0.083	-0.005

Results given in Table 7 show that vigour mean value at vineyard level is significantly different if measured on satellite or aerial imagery, if compared with uncertainty reference values (from 0.02 to 0.08) suggested in literature (Nagol et al. 2009; Borgogno-Mondino and Lessio 2015; Borgogno-Mondino et al. 2016). This was expected since the aerial-derived vigour maps are obtained by spatial interpolation after selection of vines canopy pixels, excluding any effect of background that, on the contrary, cannot be eliminated from satellite observations.

Moreover, it is worth to remind that time distance between compared aerial and satellite acquisitions ranged from 0 up to 15 days making conditions not perfectly fitting.

Nevertheless, modelling bias between SINT05 and AINT05 (Table 8 and Figure 7), it is possible to reduce such difference recovering consistency between the two datasets.

In fact, by applying calibrated regression to satellite images, differences between vineyard mean vigour values ($\Delta\mu$) can be significantly lowered below NDVI uncertainty. This fact encourages us more and more in maintaining that satellite imagery generates information consistent with the one derivable from higher resolution devices at vineyard level. Moreover, the high correlation and the effectiveness of the tested correction suggests that behind residual differences (before correction) between the two datasets there is some un-modelled effect related to atmospheric conditions and time delay between acquisitions. In operational conditions this modelling would not be possible, since aerial data to compare satellite ones with, are not available. Given this strong linear relationship we can assume that this bias, leading to different interpretation of final PMs, could be minimized and effectively absorbed during calibration of eventual regression models linking spectral indices to ground observations of biophysical parameters. In other words, we can be sure that spatial pattern of vigour from satellite or aerial datasets is consistent, while its strength, being significantly different, could bring to different results.
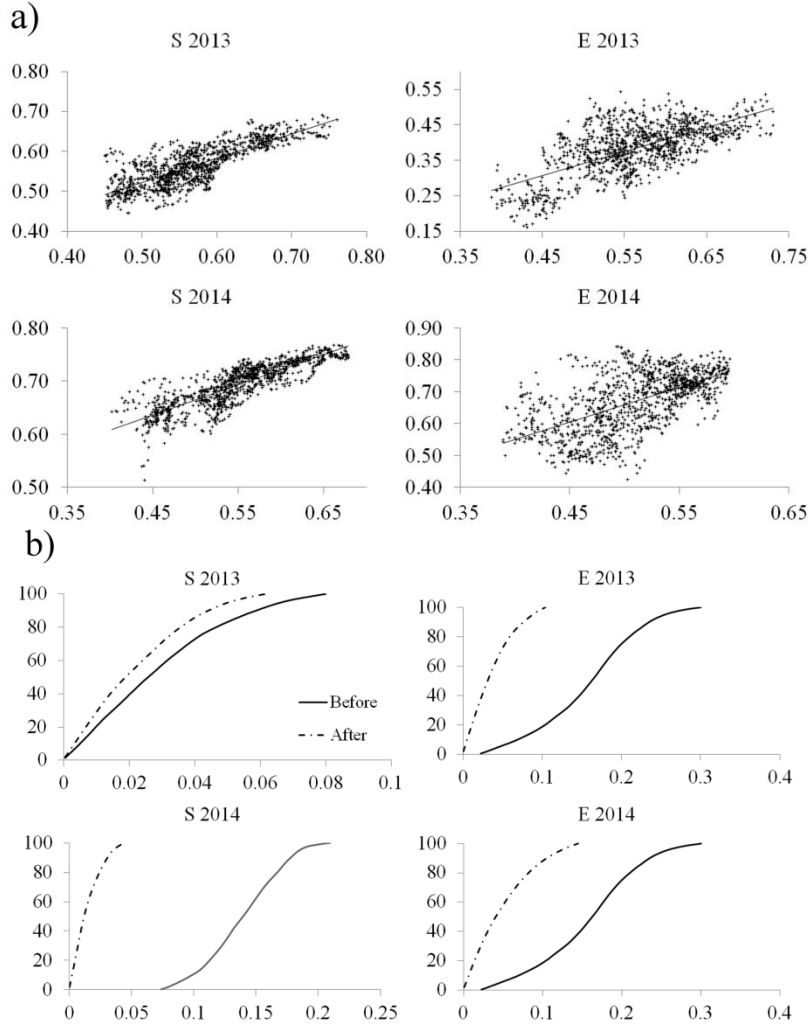
Fig. 7 (a) Scatterplots relating vigour values from satellite (x axis) and aerial (y axis) for the compared pairs of images. (b) Cumulative frequency distributions (y axis) of vigour differences (x axis) between aerial and satellite vigour values before and after bias modelling ("I and "II" like in Table 3).

Table 8 Correlation coefficients and linear regression parameters used to model vigour bias for the aerial and satellite tested image pairs ("I and "II" like in Table 3).

	I 2013	*II 2013*	*I 2014*	*II 2014*
R₄	0.81	0.67	0.85	0.60
a	0.6089	0.6760	0.5665	1.0923
b	0.2182	0.0036	0.3817	0.1130

PMs for both aerial and satellite vigour maps were obtained by cluster analysis achieved by Minimum Distance/Hill-climbing algorithm (SAGA GIS). As far as satellite maps clustering is concerned we run it both for corrected and not-corrected vigour maps, obtaining (as expected) the same result since bias modelling was linear. In all the cases we asked for 3 clusters that successively were labelled as: LOW, MEDIUM and HIGH vigour clusters. PMs are shown in Figure 8. Interpretation of clusters was achieved by calculating correspondent NDVI class mean ($\mu_{cluster}$) and standard deviation ($\sigma_{cluster}$). Results are reported in Table 9 for both aerial- and satellite-derived PMs before and after correction. A Vigour Difference coefficient (VD, see eq. 6) was defined to measure vigour distance between LOW and HIGH clusters respect

18

to the MEDIUM one. Results again demonstrates that a bias concerning vigour values from satellite is present and that, on the contrary, the spatial consistency is satisfying also at PMs level. After bias removing, VD from satellite-and aerial PMs generated more similar information. Our idea is that, thanks to its linearity, bias could be absorbed using few ground observations, in particular when a spatial modelling of physiological parameters based on spectral indices is expected. This step was not considered in this work.
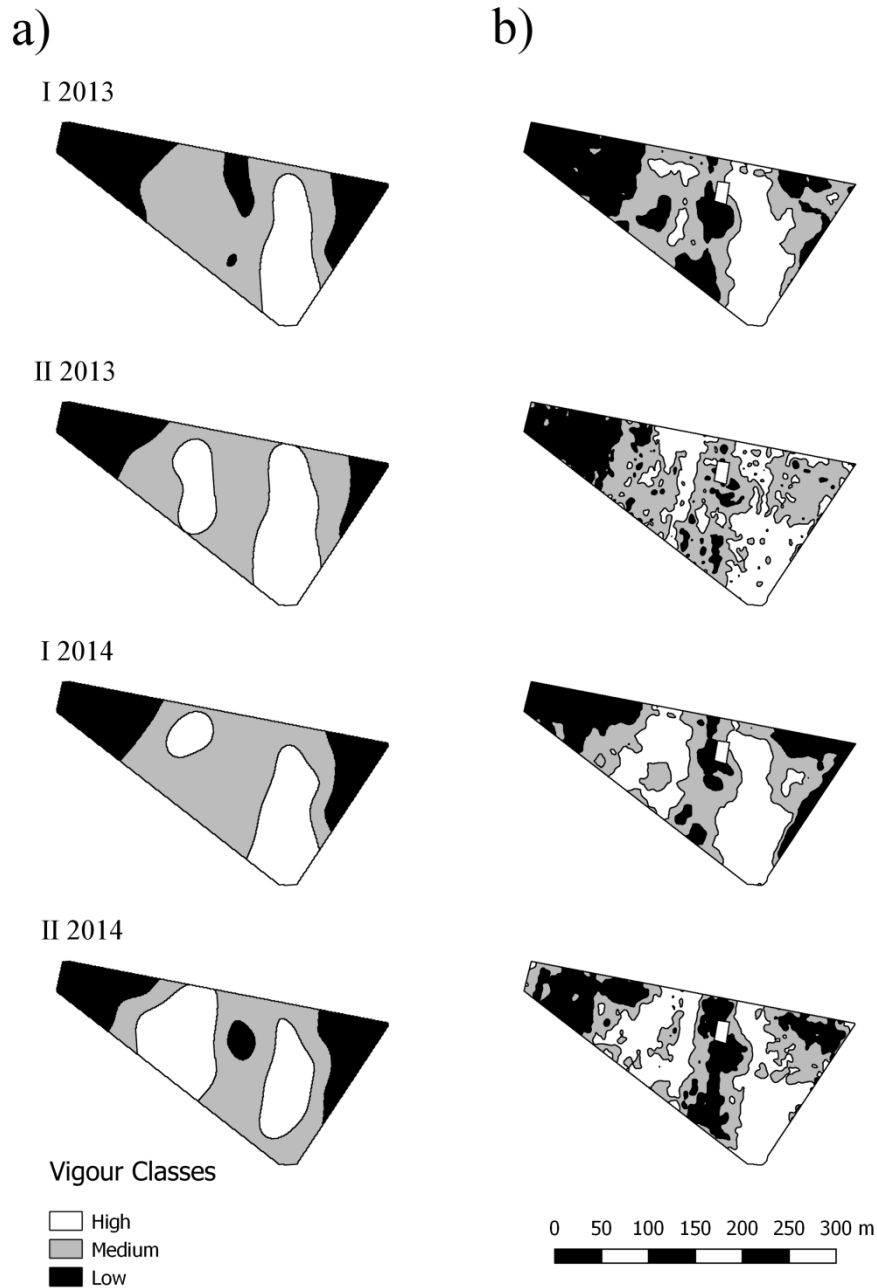
Fig. 8 Prescription maps. Satellite (a), aerial (b). Three vigour clusters (LOW, MEDIUM, HIGH) were mapped by Minimum Distance/Hill-climbing method. ("I and "II"like in Table 3).

19

Table 9 Statistic describing vigour clusters: mean, standard deviation and VD are reported for aerial PMs ("I and "II" like in Table 3).

		Aerial				
		LOW	MEDIUM	HIGH	VD (LOW) %	VD (HIGH) %
I 2013	area [%]	35.4	36.8	27.8		
	$\mu_{cluster}$	0.502	**0.564**	0.629	-10.99	11.51
	$\sigma_{cluster}$	0.021	0.018	0.023		
II 2013	area [%]	19.8	45.4	34.8		
	$\mu_{cluster}$	0.264	**0.373**	0.457	-29.19	22.52
	$\sigma_{cluster}$	0.038	0.026	0.035		
I 2014	area [%]	27.2	33.7	39.1		
	$\mu_{cluster}$	0.630	**0.684**	0.731	-8.00	6.88
	$\sigma_{cluster}$	0.024	0.016	0.015		
II 2014	area [%]	27.1	32.9	40.0		
	$\mu_{cluster}$	0.545	**0.658**	0.755	-17.07	14.75
	$\sigma_{cluster}$	0.038	0.031	0.033		

Table 10 Statistics describing vigour clusters: mean, standard deviation and VD are reported for satellite PMs before and after bias removing ("I and "II"like in Table 3).

		Satellite					Satellite corrected				
		LOW	MEDIUM	HIGH	VD (Low) %	VD (High) %	LOW	MEDIUM	HIGH	VD (LOW) %	VD (HIGH) %
I 2013	area [%]	30.6	49.0	20.3			30.6	49.0	20.3		
	$\mu_{cluster}$	0.487	**0.565**	0.669	-13.90	18.32	0.514	**0.562**	0.625	-8.54	11.21
	$\sigma_{cluster}$	0.024	0.025	0.035			0.015	0.015	0.021		
II 2013	area [%]	18.9	46.1	35.0			18.9	46.1	35.0		
	$\mu_{cluster}$	0.436	**0.540**	0.626	-19.27	15.89	0.298	**0.369**	0.427	-19.24	15.72
	$\sigma_{cluster}$	0.033	0.025	0.034			0.022	0.017	0.023		
I 2014	area [%]	24.2	50.3	25.5			24.2	50.3	25.5		
	$\mu_{cluster}$	0.458	**0.545**	0.628	-16.03	15.22	0.640	**0.690**	0.737	-7.25	6.81
	$\sigma_{cluster}$	0.025	0.022	0.026			0.014	0.012	0.015		
II 2014	area [%]	25.2	40.5	34.3			25.2	40.5	34.3		
	$\mu_{cluster}$	0.432	**0.499**	0.556	-13.33	11.44	0.585	**0.658**	0.720	-11.09	9.42
	$\sigma_{cluster}$	0.023	0.017	0.017			0.025	0.019	0.019		

Looking at the spatial size of clusters, according to Tables 7 and 8, the following features can be observed: a) in satellite derived PMs MEDIUM cluster area is always higher respect to the aerial correspondent one; b) the highest differences concern area size of HIGH clusters that, in general, satellite tends to underestimate (up to 14 %); c) size of clusters of the same type is more consistent at the end of season; d) in general, aerial PMs can map smaller parts of vineyard where, probably, vigour maxima and minima locally occur; e) cluster geometry does not change in satellite PMs operating with bias removed-vigour maps or with the original ones.

Focusing on the strength of vigour of clusters (i.e. VD values), consistency of aerial- and satellite-derived PMs is not so satisfying if no bias modeling is performed. First impression is that these differences can lead to very different considerations concerning management of agronomic corrective interventions over the vineyard. Bias removing reduce these differences, but remaining ones are still significant especially at the end of the growing season.

Further investigations could be addressed, in future, to evaluate if and how (as we hypothesize) few ground observations could help interpretation of both aerial and satellite PMs. This will lead to improve reliability of calibration of those corrective treatments aimed at making vineyard performance as much homogeneous as possible.

Conclusions

In this work we tested consistency and reliability of satellite-derived PMs respect to those that can be obtained by aerial imagery. Test design considered a vineyard of Moscato Reale sited in Apulia (South-Eastern Italy) and two growing seasons (2013 and 2014). Comparisons concerned Landsat 8 OLI images and aerial datasets from airborne RedLake MS4100 multispectral camera. We firstly investigate the role of spatial resolution in radiometric features of data and, in particular, of NDVI maps and consequently of vigour maps. We first measured the maximum expected correlation (R) between satellite- and aerial-derived spectral index maps. We found that without any pixel selection and spatial interpolation correlation ranges between 0.35 and 0.60 depending on the degree of heterogeneity of the observed surfaces. We also found that this result can be improved by operating a selection of those pixels representing vines canopy in aerial imagery and spatially interpolating them. Correlation coefficient concerning aerial *vs.* satellite vigour maps can be improved up to 0.85 (minimum 0.60), suggesting an excellent capability of satellite data to approximate aerial ones.

Using remote sensing to monitor vineyard response to agro-environmental factors in terms of vigour, with special regard to the intra-vineyard variability, has great interest for growers when reliable information and moderate costs are provided. In both the years of the present study, satellite-derived vigour maps were quite consistent with aerial-derived ones in the sample vineyard, especially concerning spatial distribution of vigour differences. The consistence of aerial-derived vigour maps with several ground observed grapevine physiological, reproductive and qualitative indices was tested in a previous study (de Palma et al. 2016), showing some good correlations. The possibility to adopt satellite images available for free, as a start point for obtaining reliable vigour maps, encourages the adoption of such technological approach in precision farming. Nevertheless, this study showed that the radiometric concerns affecting data processing (image calibration, atmospheric correction and spatial resolution of datasets) are not negligible aspects for a reliable and repeatable operational approach to remote sensing derived information for agricultural purposes. We found that the weakest point is the quantitative interpretation of mapped vigour that changes according to datasets and

21

time of acquisition. Effectiveness of bias modelling in satellite vigour maps, that was possible in our study since coeval aerial acquisitions were available, supports the idea that, only partially the quantitative interpretation of maps depends on systematic factors (e.g lightning conditions, background effects, etc.). Some others could not be directly modelled by relative comparisons between data, but probably require other auxiliary information from the field. We strongly believe that some few ground observations concerning directly NDVI measures or some other strictly related parameters (e.g LAI, LCC, etc.) are always desirable to calibrate, time to time, vigour maps from remote sensing systems. Moreover, agronomic interpretation of maps has to heavily rely on farmers experience that has to be intended as one of the main factors in the remote sensing application to the agronomic compartment.

References

Allen, R. G., Pereira, L. S., Raes, D., & Smith, M. (1998). Crop evapotranspiration-Guidelines for computing crop water requirements-FAO Irrigation and drainage paper 56. FAO, Rome, 300(9), D05109.

Arnó, J., Bordes, X., Ribes-Dasi, M., Blanco, R., Rosell, J. R., & Esteve, J. (2005). Obtaining grape yield maps and analysis of within-field variability in Raimat (Spain). *Precision Agriculture*, 5, 899-906.

Bannari, A., Morin, D., Bonn, F., & Huete, A. R. (1995). A review of vegetation indices. *Remote Sensing Reviews*, 13(1-2), 95-120.

Bramley, R. G. V. (2001). Progress in the development of precision viticulture-variation in yield, quality and soil properties in contrasting Australian vineyards (No. 14, pp. 25-43). Occasional report. http://www.cse.csiro.au/client_serv/resources/bramley1.pdf

Bramley, R., Pearse, B., & Chamberlain, P. (2003). Being profitable precisely-a case study of precision viticulture from Margaret River. *Australian and New Zealand Grapegrower and Winemaker*, 84-87.

Bramley, R. G. V., Proffitt, A. P. B., Hinze, C. J., Pearse, B., & Hamilton, R. P. (2005). Generating benefits from Precision Viticulture through selective harvesting. *Precision Agriculture*, 5, 891-898.

Borgogno-Mondino, E., & Lessio, A. (2015, July). Estimation and mapping of NDVI uncertainty from Landsat 8 OLI datasets: An operational approach. In Geoscience and Remote Sensing Symposium (IGARSS), 2015 IEEE International (pp. 629-632). IEEE. http://ieeexplore.ieee.org/stamp/stamp.jsp?arnumber=7325842

Borgogno-Mondino, E., Lessio, A., & Gomarasca, M. A. (2016). A fast operative method for NDVI uncertainty estimation and its role in vegetation analysis. *European Journal of Remote Sensing*, 49, 137-156.

Chappelle, E. W., Kim, M. S., & McMurtrey, J. E. (1992). Ratio analysis of reflectance spectra (RARS): an algorithm for the remote estimation of the concentrations of chlorophyll a, chlorophyll b, and carotenoids in soybean leaves. *Remote Sensing of Environment*, 39(3), 239-247.

22

Chavez, P. S. (1996). Image-based atmospheric corrections-revisited and improved. *Photogrammetric Engineering and Remote Sensing*, 62(9), 1025-1035.

Cook, S. E., & Bramley, R. G. V. (1998). Precision agriculture—opportunities, benefits and pitfalls of site-specific crop management in Australia. *Animal Production Science*, 38(7), 753-763.

Cortell, J. M., Sivertsen, H. K., Kennedy, J. A., & Heymann, H. (2008). Influence of vine vigor on Pinot noir fruit composition, wine chemical analysis, and wine sensory attributes. *American Journal of Enology and Viticulture*, 59(1), 1-10.

de Palma, L., Tarricone, L., Borgogno, E., Limosani, P., Paolicelli, M., Novello V. (2016). Fisiologia e qualità della produzione in Nero di Troia e Moscato Reale, in relazione alle differenze di vigore rilevate con tecniche di viticoltura di precisione. *Acta Italus Hortus,* 19, 177-178.

Delenne, C., Durrieu, S., Rabatel, G., & Deshayes, M. (2010). From pixel to vine parcel: A complete methodology for vineyard delineation and characterization using remote-sensing data. *Computers and Electronics in Agriculture,* 70(1), 78-83.

Dobrowski, S. Z., Ustin, S. L., & Wolpert, J. A. (2002). Remote estimation of vine canopy density in vertically shoot-positioned vineyards: determining optimal vegetation indices. *Australian Journal of Grape and Wine Research*, 8(2), 117-125.

Dry, P. R. (2000). Canopy management for fruitfulness. *Australian Journal of Grape and Wine Research*, 6(2), 109-115.

Fenn, R. W., Clough, S. A., Gallery, W. O., Good, R. E., Kneizys, F. X. et al. (1985). Cap.18: Optical and infrared properties of the atmosphere. In (Ed) A. S. Jursa, *Handbook of Geophysics and Space Environment.* NTIS.

Forgy, E. W. (1965). Cluster analysis of multivariate data: efficiency versus interpretability of classifications. *Biometrics*, *21*, 768-769.

Forte, L., Perrino, E. V., & Terzi, M. (2005). Le praterie a Stipa austroitalica Martinovsky ssp. austroitalica dell'Alta Murgia (Puglia) e della Murgia Materana (Basilicata). *Fitosociologia*, *42*(2), 83-103.

Frampton, W. J., Dash, J., Watmough, G., & Milton, E. J. (2013). Evaluating the capabilities of Sentinel-2 for quantitative estimation of biophysical variables in vegetation. *ISPRS Journal of Photogrammetry and Remote Sensing*, *82*, 83-92.

Gomarasca, M. A. (2009). *Basics of Geomatics.* Springer Science & Business Media.

Haboudane, D., Miller, J. R., Tremblay, N., Zarco-Tejada, P. J., & Dextraze, L. (2002). Integrated narrow-band vegetation indices for prediction of crop chlorophyll content for application to precision agriculture. *Remote Sensing of Environment*, 81(2), 416-426.

23

Hall, A., Lamb, D. W., Holzapfel, B., & Louis, J. (2002). Optical remote sensing applications in viticulture-a review. *Australian Journal of Grape and Wine Research*, 8(1), 36-47.

Hall, A., Lamb, D. W., Holzapfel, B. P., & Louis, J. P. (2011). Within-season temporal variation in correlations between vineyard canopy and winegrape composition and yield. *Precision Agriculture*, 12(1), 103-117.

Haselgrove, L., Botting, D., Heeswijck, R. V., Høj, P. B., Dry, P. R., et al. (2000). Canopy microclimate and berry composition: the effect of bunch exposure on the phenolic composition of Vitis vinifera L cv. Shiraz grape berries. *Australian Journal of Grape and Wine Research*, 6(2), 141-149.

Jackson, R. S. (2008). *Wine science: principles and applications*. Academic press.

Johnson, L. F., Bosch, D. F., Williams, D. C., & Lobitz, B. M. (2001). Remote sensing of vineyard management zones: Implications for wine quality. *Applied Engineering in Agriculture*, 17(4), 557-560.

Johnson, L. F., Roczen, D. E., Youkhana, S. K., Nemani, R. R., & Bosch, D. F. (2003). Mapping vineyard leaf area with multispectral satellite imagery. *Computers and Electronics in Agriculture*, 38(1), 33-44.

Johnson, L. F. (2003). Temporal stability of an NDVI-LAI relationship in a Napa Valley vineyard. Australian *Journal of Grape and Wine Research*, 9(2), 96-101.

King, P. D., Smart, R. E., & McClellan, D. J. (2014). Within-vineyard variability in vine vegetative growth, yield, and fruit and wine composition of Cabernet Sauvignon in Hawke's Bay, New Zealand. *Australian Journal of Grape and Wine Research*, 20(2), 234-246.

Lanjeri, S., Melia, J., & Segarra, D. (2001). A multi-temporal masking classification method for vineyard monitoring in central Spain. *International Journal of Remote Sensing*, 22(16), 3167-3186.

Malenovský, Z., Rott, H., Cihlar, J., Schaepman, M. E., García-Santos, et al. (2012). Sentinels for science: Potential of Sentinel-1,-2, and-3 missions for scientific observations of ocean, cryosphere, and land. *Remote Sensing of Environment*, 120, 91-101.

Matese, A., Toscano, P., Di Gennaro, S. F., Genesio, L., Vaccari, et al. (2015). Intercomparison of UAV, aircraft and satellite remote sensing platforms for precision viticulture. *Remote Sensing*, 7(3), 2971-2990.

Montero, F. J., Melia, J., Brasa, A., Segarra, D., Cuesta, A., & Lanjeri, S. (1999). Assessment of vine development according to available water resources by using remote sensing in La Mancha, Spain. *Agricultural Water Management*, 40(2), 363-375.

Moran, M. S., Jackson, R. D., Slater, P. N., & Teillet, P. M. (1992). Evaluation of simplified procedures for retrieval of land surface reflectance factors from satellite sensor output. *Remote Sensing of Environment*, 41(2-3), 169-184.

Moran, M. S., Vidal, A., Troufleau, D., Qi, J., Clarke, T. R., et al. (1997). Combining multifrequency microwave and optical data for crop management. *Remote Sensing of Environment*, 61(1), 96-109.

24

Nagol, J. R., Vermote, E. F., & Prince, S. D. (2009). Effects of atmospheric variation on AVHRR NDVI data. *Remote Sensing of Environment*, 113(2), 392-397.

Petrie, P. R., Trought, M. C., & Howell, G. S. (2000). Fruit composition and ripening of Pinot Noir (Vitis vinifera L.) in relation to leaf area. *Australian Journal of Grape and Wine Research*, 6(1), 46-51.

Pinter Jr, P. J., Hatfield, J. L., Schepers, J. S., Barnes, E. M., Moran, et al. (2003). Remote sensing for crop management. *Photogrammetric Engineering & Remote Sensing*, 69(6), 647-664.

Price, J. C., & Bausch, W. C. (1995). Leaf area index estimation from visible and near-infrared reflectance data. *Remote Sensing of Environment*, 52(1), 55-65.

Proffitt, T., & Proffitt, A. P. B. (2006). Precision viticulture: a new era in vineyard management and wine production (pp. 49-55). Adelaide: Winetitles.

Read, J. J., Tarpley, L., McKinion, J. M., & Reddy, K. R. (2002). Narrow-waveband reflectance ratios for remote estimation of nitrogen status in cotton. *Journal of Environmental Quality*, 31(5), 1442-1452.

Rey, C., Martín, M. P., Lobo, A., Luna, I., Diago, M. P., et al. (2013). Multispectral imagery acquired from a UAV to assess the spatial variability of a Tempranillo vineyard. *Precision Agriculture'13*, 617-624. Wageningen Academic Publishers.

Rubin, J. (1967). Optimal classification into groups: an approach for solving the taxonomy problem. *Journal of Theoretical Biology*, 15(1), 103-144.

Romero, P., Gil-Muñoz, R., del Amor, F. M., Valdés, E., Fernández, J. I., & Martinez-Cutillas, A. (2013). Regulated deficit irrigation based upon optimum water status improves phenolic composition in Monastrell grapes and wines. *Agricultural Water Management*, 121, 85-101.

Sibanda, M., Mutanga, O., & Rouget, M. (2015). Examining the potential of Sentinel-2 MSI spectral resolution in quantifying above ground biomass across different fertilizer treatments. *ISPRS Journal of Photogrammetry and Remote Sensing*, 110, 55-65.

Song, J., Smart, R. E., Dambergs, R. G., Sparrow, A. M., Wells, R. B., et al. (2014). Pinot Noir wine composition from different vine vigour zones classified by remote imaging technology. *Food Chemistry*, 153, 52-59.

Tagarakis, A., Liakos, V., Fountas, S., Koundouras, S., & Gemtos, T. A. (2013). Management zones delineation using fuzzy clustering techniques in grapevines. *Precision Agriculture*, 14(1), 18-39.

Tarini, M., Cignoni, P., & Montani, C. (2006). Ambient occlusion and edge cueing for enhancing real time molecular visualization. *IEEE Transactions on Visualization and Computer Graphics*, 12(5).

Testa, S., Mondino, E. C. B., & Pedroli, C. (2014). Correcting MODIS 16-day composite NDVI time-series with actual acquisition dates. *European Journal of Remote Sensing*, 47, 285-305.

25

Thenkabail, P. S. (2003). Biophysical and yield information for precision farming from near-real-time and historical Landsat TM images. *International Journal of Remote Sensing*, 24(14), 2879-2904.

Winkler, A. J. (1974). *General Viticulture*. University of California Press.

Yu, K., Lenz-Wiedemann, V., Leufen, G., Hunsche, M., Noga, G., et al. (2012). Assessing hyperspectral vegetation indices for estimating leaf chlorophyll concentration of summer barley. *ISPRS Annals of the Photogrammetry, Remote Sensing and Spatial Information Sciences*, 89-94.

Zhang, X., Yan, G., Li, Q., Li, Z. L., Wan, H., & Guo, Z. (2006). Evaluating the fraction of vegetation cover based on NDVI spatial scale correction model. *International Journal of Remote Sensing*, 27(24), 5359-5372.

Web References

Earth Explorer. Free satellite multi-spectral image datasets*: http://earthexplorer.usgs.gov/* - Last accessed 13 February 2017.

Grass GIS. Grass GIS 6.5svn Reference Manual*: http://semiautomaticclassificationmanual-it.readthedocs.io/it/latest/Landsat_conversion.html* – Last accessed 13 February 2017.

Landsat 8 Data Users Handbook:

https://landsat.usgs.gov/sites/default/files/document/Landsat8DataUsersHandbook.pdf – Last accessed 13 February 2017.

TerraSystem: *http://www.terrasystem.it/en/index.htm* – Last accessed 13 February 2017.